Astron. Astrophys. 264, 654–660 (1992)

ASTRONOMY AND ASTROPHYSICS

X-ray spectroscopy of the young supernova remnant RCW 86

J.S. Kaastra[1], **I. Asaoka**[2,3], **K. Koyama**[4], **and S. Yamauchi**[2]

[1] SRON Laboratory for Space Research, P.O. Box 9504, 2300 RA Leiden, The Netherlands
[2] Department of Astrophysics, School of Science, Nagoya University, Furo-cho, Chikusaku, Nagoya 464-01, Japan
[3] Present address: Max Planck Institut für Extraterrestrische Physik, Giessenbachstrasse, W-8046 Garching, Germany
[4] Department of Physics, Faculty of Science, Kyoto University, Sakyo-ku, Kyoto 606-01, Japan

Received December 24, 1991; accepted April 16, 1992

Abstract. An X-ray spectrum of the bright supernova remnant RCW 86 taken by the Japanese X-ray satellite Ginga is analysed with non-equilibrium ionisation models. The spectrum, after correction for galactic ridge emission, is consistent with a type II supernova explosion. From the identification with the historical remnant of A.D. 185 a distance of 0.95 ± 0.4 kpc is derived. The massive progenitor had a mass of at least $22 M_{\odot}$, and went off in a medium modified by its stellar wind with an explosion energy of $2\,10^{44}$ J. The abundances of Si, S and Fe are below the solar abundances: 0.7, 0.7 and 0.2 respectively.

Key words: supernovae and supernova remnants: general – supernovae and supernova remnants: RCW 86 – X-rays: spectroscopy

1. Introduction

RCW 86 (alias MSH 14-63, G 315.4-2.3, PKS 1439-62, Cen XR-1, 1H 1438-623) is one of the brightest X-ray supernova remnants. It was identified as the remnant of the historical supernova of A.D. 185 by Clark & Stephenson (1977), although there may be some doubt about this identification (Huang & Moriarty-Schieven 1987). X-ray images taken by the Einstein IPC and HRI detectors (Pisarski et al. 1984) and by the Exosat LE detector (Claas et al. 1989) show a shell-like structure with strongly enhanced emission in the SW part of the remnant. X-ray spectra taken by the Apollo–Soyuz mission (Naranan et al. 1977) showed the presence of thermal bremsstrahlung. Winkler (1978) needed two temperature components (0.22 keV and >5 keV) to explain the X-ray spectrum observed by OSO-7. This most probably does not reflect a true double temperature structure, but merely non-equilibrium ionisation (NEI) effects. Fits with such NEI models were done by Nugent et al. (1984) using data from the HEAO-1 A2 experiment. However all of these previous spectra are contaminated by X-ray emission from the galactic ridge as was shown by Claas et al. (1989). These authors studied the Exosat LE and ME detector spectra of RCW 86, corrected for the emission from the galactic ridge. They were unable to determine the ionisation parameter $U \equiv \int n_e \, dt$ from the spectrum. Therefore, they assumed the NE part of the remnant to be in a Sedov phase and derived several parameters of the progenitor. Based upon the Sedov assumption, they argued that RCW 86 is most probably the result of a type I supernova.

In this paper we present the analysis of new spectral data obtained by the Japanese X-ray satellite Ginga. This analysis allows a direct determination of U and of the abundances of a few elements. These data strongly favour a type II supernova, as will be shown in Sect. 3.

2. Observations

The present X-ray spectrum of RCW 86 was obtained by the Large Area Counter (LAC) on the third Japanese X-ray astronomy satellite *Ginga*. The LAC comprises eight multi-cell proportional counters with a total effective area of 4000 cm^2. The coarse gain amplifier of the detector has two settings, low (CG-L) and high (CG-H). Most observations were performed in the CG-L mode, but in this case the CG-H mode was used. The advantage of CG-H over CG-L is an energy sampling which is a factor of 2 better. A disadvantage is that the energy is not limited to the usual 0.5–37 keV range, but to 0.25–18.7 keV. Therefore, the fluorescent silver line at 22.1 keV caused by the collimator which is usually used to check the gain calibration cannot be used for CG-H. However since the gain of the detector appears to be very stable this is not a serious problem. We checked the gain stability by analysing a Cas A observation obtained in the CG-H mode. A fit to that spectrum reproduced the line centroid of the iron line at 6.6 keV (Jansen et al. 1988) to within the statistical errors (0.5%). The energy resolution of the detector is 18% at 6 keV, and scales as $E^{-0.5}$ over the full energy range. The detector has a field of view of $1° \times 2°$ full width at half maximum, and was used in the MPC-1 mode with a time resolution of 16 s. More details about the instrument are given by Turner et al. (1989). A full discussion about the background determination method is given by Hayashida et al. (1989).

RCW 86 was observed during the PV phase of Ginga from August 15–16, 1987, with an effective exposure time of 22000 s. The pointing was centered at $l_{II} = 315\overset{\circ}{.}17$, $b_{II} = -2\overset{\circ}{.}76$ (we will use galactic coordinates throughout, since the galactic plane plays an important role in the subsequent analysis). This is about half a degree offset from the centre of the remnant. The detectors consist of two layers, called top and mid layer. We used only data from the top layer, since the mid layer is mostly sensitive to X-ray photons above 10 keV and RCW 86 has no high count rate above 10 keV. The criteria used for inclusion of the data in our spectral

Send offprint requests to: J.S. Kaastra

analysis were (more details and definitions are given by Hayashida et al. (1989):

(1) charged particle cutoff-rigidity ≥ 9 GeV/c;

(2) Earth elevation angle $\geq 5°$;

(3) first and last bin before and after detector switches were omitted;

(4) data with sudden changes of the SUD (surplus over upper discriminator) larger than 3σ were rejected;

(5) data from orbits passing through the South Atlantic Anomaly, as well as the first orbit after passage were rejected.

The background data were obtained from a CG-H observation of a blank field centered at $l_{II}=329.^{\circ}74$, $b_{II}=-5.^{\circ}57$ observed at August 20, 1987. A background observation obtained immediately after the RCW 86 observation on August 17 could not be used since it was centered at $l_{II}=317.^{\circ}46$, $b_{II}=-0.^{\circ}44$ i.e. very close to the galactic plane. It is well known (e.g. Warwick et al. 1985) that near the galactic plane a considerable emission component from the galactic ridge is present. Moreover, the Exosat map of Warwick et al. as well as a Ginga scan along the galactic plane show the presence of an extra source at about $l_{II}=317.^{\circ}2$, $b_{II}=+0.^{\circ}3$ within the August 17 pointing. The August 20 background is free from galactic ridge contamination.

The RCW 86 pointing itself is not completely free from galactic ridge contamination. We have corrected the spectrum as follows. Yamauchi (1991) has shown that the galactic ridge emission as observed by Ginga can be modelled by a disk with a radius R of 5.7 kpc and a constant emissivity within R when integrated over z. The z-dependence of the emissivity is exponential $\sim\exp(-|z/z_s|)$ with a scale height z_s of 120 pc. The distance towards the galactic centre is taken as 8.5 kpc. At the galactic longitude of RCW 86 this leads to an apparent exponential scale height b_s in galactic latitude of $1.1\pm0.1°$, taking the estimated uncertainties into account. The spectrum of the galactic ridge contains an iron emission line and most likely has a thermal origin (Koyama et al. 1986). A spectrum of the galactic ridge near RCW 86 obtained during a scanning observation ($l_{II}=315°.2$, $b_{II}=+0°.2$) and fitted by a thermal equilibrium plasma model (Masai 1984) yielded an acceptable fit ($\chi^2_{15}=12.5$) with a temperature of 8.1 ± 1.7 keV, an iron abundance of 0.49 ± 0.23 (in solar units), and an absorbing column density N_H of $\log N_H(\mathrm{cm}^{-2})=21.7\pm0.3$. Using the exponential model outlined above we estimated the contribution of the ridge to the RCW 86 spectrum to be a fraction 0.162 ± 0.029 of the ridge spectrum presented above. The final RCW 86 spectrum was now obtained by using the raw spectrum measured on August 15–16 (containing ridge contamination), correcting for the background using the blank sky observation of August 20, and finally subtracting the ridge contribution determined as described above. The ridge correction relative to the clean RCW 86 spectrum ranges from 1.5% near 1 keV to 22% near 15 keV.

A second correction to the spectrum arises from the extended size of the remnant (radius 21′) as compared to the collimator. As described by Turner et al. (1989) the inner structure of the collimator is somewhat reflective to X-rays below 6 keV. Especially for off-axis sources X-ray reflection leads to an increased soft X-ray flux. We corrected for this effect by assuming that the X-ray flux of RCW 86 as observed by Ginga is spatially distributed like the Einstein IPC image obtained in the 0.6–4.5 keV range. The correction can be as large as 15% at 2.7 keV. The correction was not applied to the X-ray spectrum but to the response matrix.

Figure 1 shows the contribution of various components to the total statistical uncertainty of the spectrum. Included is the Poisson noise of both the source and the background observation, a systematic error of 1% of the raw background spectrum, the uncertainty in the galactic ridge correction and the uncertainty due to the reflection correction. Below 2 keV the observational error is dominated by the Poisson noise of the background observation, between 2 and 7 keV the galactic ridge correction is the main source of uncertainty and above 7 keV the background dominates the error again.

3. Spectral analysis

The spectrum of RCW 86 obtained by the method described in Sect. 2 was fitted in the energy range 1.16–16.8 keV. We used the set of models of Kaastra & Jansen (1992). These models allow for self-similar hydrodynamical models both with and without a reverse shock, and with adiabatic, isothermal or isentropic equations of state, with various interstellar and stellar ejecta density distributions. The undisturbed interstellar density is modelled by a power law $\rho\propto r^{-s}$ and the undisturbed stellar ejecta by a power law $\rho\propto r^{-n}$. Included among others are the classical Sedov model and Chevalier's reverse shock models. The corresponding plasma code takes non-equilibrium effects into account and includes the emission from 15 chemical elements (H, He, C, N, O, Ne, Na, Mg, Al, Si, S, Ar, Ca, Fe and Ni).

The calculation method for the model spectra as discussed by Kaastra & Jansen is as follows. First the hydrodynamical model is calculated. The remnant is divided into several shells (we used

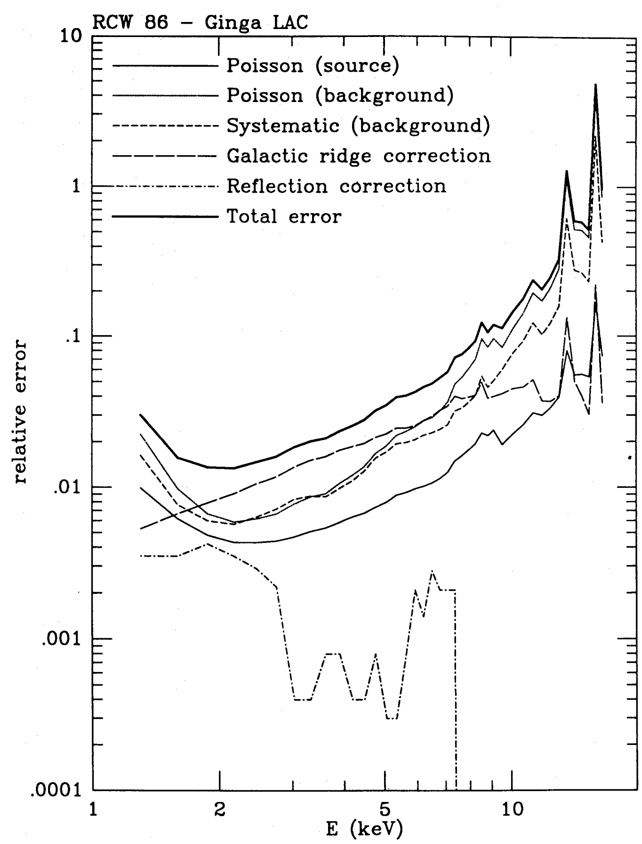

Fig. 1. Various contributions to the relative errors of the spectrum as a function of energy

25 shells in the present case), and for each shell the position, velocity, density and temperature as a function of time is determined. Using this plasma history, the time evolution of the ion concentrations is calculated for each shell, using eigenvalue decomposition of the ionisation–recombination transition matrix. The transition matrix depends only upon temperature for low density plasmas like SNRs, hence the eigenvalues and eigenvectors are precalculated, stored on computer disk and interpolated where necessary. Given the ion concentrations and final temperature of each shell, the X-ray spectrum is calculated, including more than 2400 spectral lines and free-free, free-bound and two-photon continuum emission. For a full description, we refer to Kaastra & Jansen (1992).

As a first step, we fitted the spectrum by a simple $n_e t$ model (Fig. 2 and Table 1). This model has only one component: a plasma with a constant temperature and density, which at $t=0$ is instantaneously heated from a very low temperature to its current value. The model is characterised by 4 parameters: the apparent main shock angular radius θ, the reduced emission measure $C \equiv \int n_e n_H \, dV/d^2$, the emission measure averaged electron temperature $T \equiv \int n_e n_H T_e \, dV / \int n_e n_H \, dV$ and the emission measure averaged ionisation parameter $U \equiv \int n_e n_H [\int n_e(t) \, dt] \, dV / \int n_e n_H \, dV$. Here n_e and n_H are the local electron and hydrogen density, V is the emitting volume and d is the distance to the remnant. The integration over time t in the expression for U is for a fixed mass element. Furthermore, the 15 elemental abundances are free parameters, as well as the interstellar galactic column density. The interstellar absorption cross section was taken from Morrison & McCammon (1983). Not all the 15 chemical elements show significant line emission in the present spectrum. In order to reduce the number of free parameters in our fit, we have fixed all abundances to their solar values (Anders & Grevesse 1989), unless it was possible to determine their abundance with sufficient accuracy. This left us essentially with Si, S, Ar and Fe as free parameters. The results of our fit are shown in Table 1. The errors shown are one sigma errors for 1 interesting parameter (corresponding to an increase in χ^2 of 2 if the interesting parameter is fixed but all other parameters remain free). Only the errors of the parameters for the $n_e t$ model are shown in the table; the relative errors in the other models were very similar and thus the absolute errors for the other models can be estimated easily from Table 1.

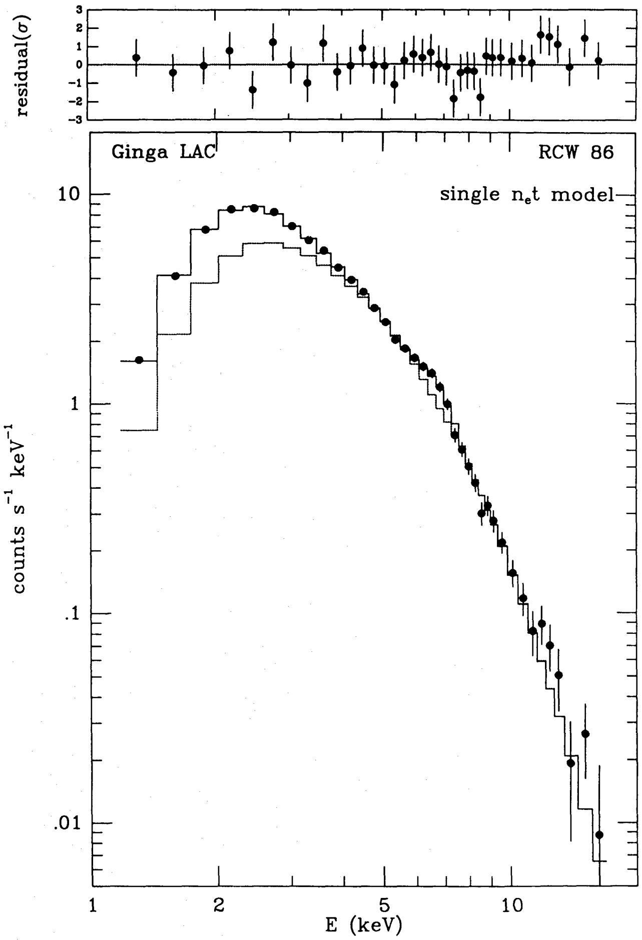

Fig. 2. Spectrum of RCW 86 fitted to a simple $n_e t$ model as described in the text. The solid line indicates the best fitting model (continuum plus lines), the dashed line the continuum contribution only

We have only obtained an upper limit to the interstellar column density. This is no surprise since Ginga is not sensitive to X-rays below 1 keV. The present temperature (4.3 keV) is slightly higher than the temperature obtained by Exosat (3.4 ± 0.2 keV,

Table 1. Spectral fits. Parameters in ( ) were kept fixed. Abundances are in solar units

Parameter	$n_e t$ model	Sedov	Chevalier	Sedov	Chevalier	Band	Solinger
χ^2	26.21	25.18	24.51	25.41	22.86	29.63	26.89
Degrees of freedom	30	30	30	30	30	30	30
s	—	(0)	(0)	(2)	(2)	(2)	(0)
n	—	—	(7)	—	(12)	(12)	—
θ(′)	—	(21)	(21)	(21)	(21)	(21)	(21)
$C\,(10^{56}\,m^{-3}\,pc^{-2})$	16.3	17.2	11.2	18.6	19.2	5.2	16.6
T(keV)	4.31 ± 0.23	4.27	5.05	3.92	3.93	4.16	4.24
$U\,(10^{16}\,m^{-3}\,s)$	8.1 ± 2.5	9.9	13.8	21.5	21.8	27.3	9.3
$N_H\,(10^{24}\,m^{-2})$	0 (< 24)	0	0	0	0	0	0.2
Si	0.59 ± 0.07	0.64	0.63	0.73	0.74	0.80	0.58
S	0.62 ± 0.07	0.64	0.60	0.76	0.75	0.88	0.67
Ar	1.33 ± 0.35	1.28	1.08	1.42	1.30	1.74	1.43
Fe	0.18 ± 0.05	0.20	0.21	0.18	0.19	0.20	0.18

Claas et al. 1989); however in the latter case a two temperature equilibrium model was used, while we used a single component non-equilibrium model. Moreover, the present Ginga data are biased towards the SW part of the remnant due to the pointing direction, while the Exosat spectrum represents better the complete remnant. HEAO-1 (Nugent et al. 1984) detected a much higher temperature (5.1 keV), but in that case there should be considerable contamination from both the Galactic ridge, and other contaminating sources near the galactic ridge like the one detected in the scanning mode of Ginga (see before), since HEAO-1 had a rather wide field of view (collimator 3° × 3° FWHM). For the same reason, the derived strength and the line energy of the Fe Kα line as detected by HEAO-1 are probably contaminated.

The emission normalisation constant as derived from the Exosat (Claas et al. 1989) and Einstein (Pisarski et al. 1984) data are both $C = 11.0$, while HEAO-1 obtains $C = 12.7$. C is expressed in units of $10^{56}\ \mathrm{m}^{-3}\ \mathrm{pc}^{-2}$ throughout this paper. However Ginga did not detect all the flux of RCW 86, due to the finite field of view of Ginga and the fact that the pointing was offset half a degree from the centre of the remnant towards the south. The observed normalisation constant is therefore merely a lower limit. If the X-ray emission observed by Ginga has the same distribution as the Einstein IPC image in the 0.6–4.5 keV range, we obtain an effective collimation efficiency f_{col} of 0.391. The collimation efficiency is defined here as the measured flux/true flux. If instead we had chosen the Exosat LE image below 2 keV we would have obtained $f_{\mathrm{col}} = 0.417$. Since the IPC image has better statistics and coincides better with the Ginga detector energy range than the LE image, we will adopt $f_{\mathrm{col}} = 0.391 \pm 0.026$. Using this value, we obtain the true reduced emission measure $C = 16.3 \pm 1.0$ listed in Table 1. At a first glance this seems to be inconsistent with the Exosat and Einstein emission measure; however, the estimate of C depends upon the adopted temperature and spectral model. C is essentially determined by the X-ray flux F_{X} and $F_{\mathrm{X}} \propto C T^{0.5}$ for high temperatures; since Exosat and Einstein assumed temperatures of 3.4 and 1.2 keV respectively, their emission measures corrected to the present Ginga temperature should be considerably larger than the values quoted above.

The present Ginga spectrum yields directly an accurate measurement of the ionisation parameter U. From the X-ray images we also know the angular shock radius: $21 \pm 1'$ (Claas et al. 1989). So we have a complete knowledge of the 4 basic parameters (θ, C, T and U). It is known that the X-ray spectrum corresponding to more sophisticated hydrodynamical models can also be described in first approximation with this same set of 4 parameters (Hamilton & Sarazin 1984; Kaastra & Jansen 1992; and compare the fit to the Chevalier model discussed below). But given the set of 4 parameters and a hydrodynamical model, one can calculate the distance and age of the remnant. As described in the introduction, the generally accepted age of RCW 86 is 1800 yr, and its distance is somewhere between 0.7 and 3.2 kpc (as summarised by Claas et al. 1989). Then by comparing the calculated age or distance to the true values, we can exclude several hydrodynamical models.

There is one caveat to this method, however. The hydrodynamical models used have spherical symmetry, while the X-ray emission from RCW 86 has not; there is much more flux in the SW part than in the NE part. This asymmetry may be caused by different scenario's: inhomogeneous ejection by the progenitor star, or an inhomogeneous interstellar medium. Since our observed spectrum is strongly biased towards the bright SW part, we introduce a filling factor f defined by the ratio of the observed flux of RCW 86 to the flux of a remnant with uniform emissivity as strong as the SW part. Clearly, $f < 1$. It is possible to make a rough estimate of f from the Einstein and Exosat X-ray images. Adopting polar coordinates (r, ϕ) in the plane of the sky we calculate the radially integrated intensity $I(\phi) \equiv \int I(r, \phi) r\, dr$. In Fig. 3 we show $I(\phi)$ as determined from the Einstein image, as well as $I(\phi)$ convolved with the Ginga collimator response. The full width at half maximum of $I(\phi)$ is about 70°. If we approximate the SW part by the intersection of a cone-like structure with a thin spherical shell and adopt a half-opening angle θ of $70/2 = 35°$, we get a filling factor f of about 10%. On the other hand, assuming that the SW part resembles more an elongated filament, we estimate a filling factor of 1%. Hence we assume that f is typically in the range 0.01–0.1. In our following spectral fits we will derive the filling factor f from the observed value of C by fixing the age of the remnant to 1800 yr.

As the next step we fit the spectrum with several hydrodynamical models. The model of Chevalier (1982) describes a self-similar adiabatic shock moving into a medium with interstellar density $\rho \propto r^{-s}$. In addition there is a reverse shock in the shocked stellar ejecta. The stellar ejecta have a pre-shock density distribution $\rho \propto r^{-n}$. The Sedov model (1959) is similar to Chevalier's model but does not contain a reverse shock (and no stellar ejecta). Note that the Sedov model is formally equal to Chevalier's model in the limit of $n \to 5$. The isothermal model of Band (1988) also contains both a main shock running into the interstellar medium as well as

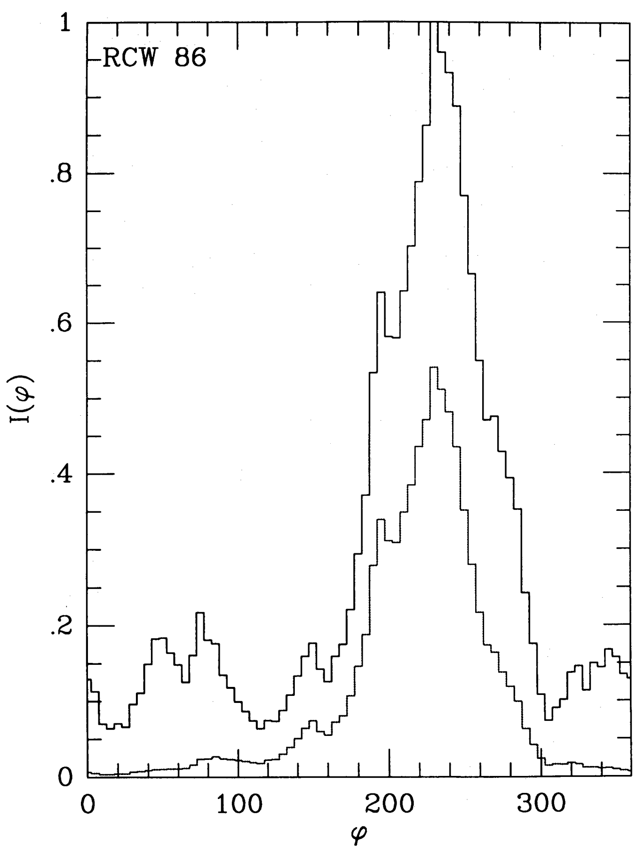

Fig. 3. Radially integrated brightness distribution of RCW 86, obtained from the Einstein IPC image (solid line). The dashed line was obtained from the same image but convolved with the Ginga collimator response

a reverse shock in the stellar ejecta. The isothermal model of Solinger et al. (1975) does not contain a reverse shock. The results of the spectral fitting are shown in Table 1. The normalisation C listed is the reduced emission measure of the shocked interstellar medium component (without the ejecta contribution), corrected for the collimator correction discussed before. The errors on the fitting parameters are very similar to the errors of the simple $n_e t$ model discussed before and are omitted therefore from Table 1. In Table 2 we show the parameters deduced from the models in Table 1. Again the errors shown are one sigma errors, and they are only shown for the Chevalier $s=2$, $n=12$ model; for the other models, the relative errors are similar to the errors in Chevalier's model, since the same scaling laws are used and the relative errors in the fitted spectral parameters of Table 1 are also similar.

For Chevalier's model with $s=0$ (homogeneous interstellar medium) it was only possible to obtain acceptable fits for n smaller than about 7. For larger values of n, the emission measure of the shocked ejecta becomes so high that the spectrum resembles a high temperature spectrum with a strong soft excess; such an excess is not observed in the present spectrum. However, the deduced filling factor f for the $s=0$ models is rather small (<0.0063) which is hardly consistent to the value derived before from the X-ray image. Taking into account the observational uncertainty of $\sim 50\%$ in f does not alter this conclusion. Moreover, even if $f \sim 0.01$, not inconsistent with the X-ray image, there is an internal inconsistency: for $f=0.01$, RCW 86 should have the structure of an elongated filament, clearly in contradiction with the assumptions behind the hydrodynamical model (spherical symmetry; the thickness of the filament is much smaller than the distance to the explosion centre). A filling factor of ~ 0.1 on the other hand would imply a structure sustaining a solid angle of about 1 steradian, locally more in accordance with the assumptions behind a spherical symmetric model.

The isothermal model of Solinger et al. which does not contain a reverse shock yields an acceptable fit for s in the range of 0–2. However, the explosion energy for $s=2$ of only 0.003 10^{43} J is unrealistically small. For $s=0$ the explosion energy is larger. Although most parameters of the isothermal $s=0$ model are realistic, the filling factor of 0.0078 (Table 2) is perhaps too low (see the discussion above for Chevalier's $s=0$ models).

Band's isothermal model also yields acceptable fits, however the deduced explosion energy and ejected mass are unrealistically high. As an example, the best fitting $s=2$, $n=12$ isothermal Band model is listed in Tables 1 and 2. Also for other sets of parameters (with higher but still acceptable χ^2-values) no realistic hydrodynamical parameters could be derived for Band's model: either the ejected mass is larger than $1000 M_\odot$, or the filling factor is larger than 1. We conclude that RCW 86 is not well modelled by an isothermal Band model with a reverse shock.

Chevalier's model with $s=2$ yields acceptable fits for all values of n. The χ^2 values differ by no more than 2.5. In this case the filling factor values derived are consistent with the value from the X-ray image. We have fitted models with several values of n, but we found the best results for n close to 12. Hence we will adopt the Chevalier model with $s=2$ and $n=12$ as our best fit, although we cannot exclude $n=5$ (the Sedov limit). A plot of the spectrum is shown in Fig. 4. The χ^2 value of the current fit (22.86) is even lower than for the simple $n_e t$ model (26.21).

The distance derived from Chevalier's model (0.8 ± 0.4 kpc) is in good agreement with distances derived by other methods (e.g. 1 kpc, derived from optical line ratio's: Ruiz 1981).

The large value of the ejected mass ($34 \pm 23 M_\odot$) as well as the fact that we obtain the best agreement with $s=2$, $n=12$ both indicate that RCW 86 was probably the result of a type II supernova explosion. Also the derived explosion energy of (2.2 ± 1.5) 10^{44} J is consistent with what is usually assumed for a type II explosion.

The abundances in RCW 86 are clearly non-solar for at least 3 elements. Both Si and S are underabundant: about 75% of the solar value. Iron is even more underabundant: it has an abundance of only 19% of the solar value. The abundances derived are nearly independent of the adopted hydrodynamical model, as Table 1 clearly shows. We note that in our best model (the Chevalier $s=0$, $n=12$ model) essentially all X-ray emission is caused by the shocked interstellar medium: the shocked stellar ejecta are much cooler. Hence the abundances measured are essentially the abundances in the pre-supernova stellar wind. A low iron abundance for RCW 86 as compared to other young remnants (Kepler, RCW 103) was also found from an analysis of optical Fe II and Fe III emission (Leibowitz & Danziger 1983).

Table 2. Parameters deduced adopting an age of 1800 yr

Model	Sedov	Chevalier	Sedov	Chevalier	Band	Solinger
s	0	0	2	2	2	0
n	—	7	—	12	12	—
Filling factor f	0.0063	0.0024	0.023	0.063 ± 0.028	0.013	0.0078
Distance (kpc)	1.3	1.0	1.0	0.8 ± 0.4	1.6	0.7
Interstellar n_H (cm^{-3})	1.8	2.2	0.51	0.24 ± 0.08	0.016	2.6
E_0 (10^{44} J)	5.0	4.7	1.7	2.2 ± 1.5	990	2.3
Swept-up mass ($M_\odot$)	116	68	46	13 ± 9	995	28
Ejected mass ($M_\odot$)	—	34	—	34 ± 23	4430	—
Shocked ejecta T (keV)	—	2.16	—	0.041	4.16	—
Shocked ejecta U (10^{16} m^{-3} s)	—	24	—	970	17	—
Shocked ejecta C (10^{56} m^{-3} pc^{-2})	—	9.4	—	3050	15.6	—
Reverse shock radius	—	0.792	—	0.805	0.974	—
contact surface radius	—	0.847	—	0.816	0.997	—

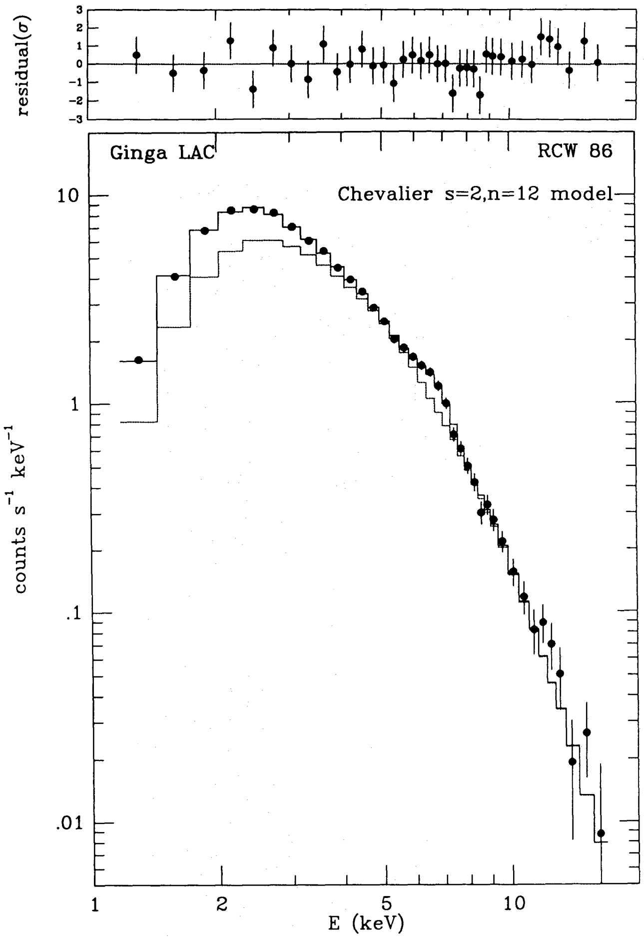

Fig. 4. Spectrum of RCW 86 fitted to a Chevalier $s=2$, $n=12$ model. The solid line indicates the best fitting model (continuum plus lines), the dashed line the continuum contribution only

From an analysis of the optical filaments, Ruiz (1981) obtained typical sulphur abundances of 0.25–0.5, also less than solar. The typical density and temperature of these filaments as derived by Ruiz (100 cm^{-3} and 10^5 K) are close to what our best fit Chevalier model predicts for the shocked stellar ejecta: about 80 cm^{-3} and 4 10^5 K respectively.

We have checked the influence of the galactic ridge correction on the derived elemental abundances. In the extreme case of no galactic ridge correction at all, we found for the simple $n_e t$ model that the abundances and U do not change more than a few %. The main effect is an apparent increase of the temperature from 4.31 to 4.81 keV.

Finally, we consider the asymmetry of the X-ray image of RCW 86. The SW part is on average about 5 times brighter than the NE part of the remnant (Fig. 3). Such an asymmetry can be caused by various mechanisms: e.g. inhomogeneous ejection of matter, or an inhomogeneous interstellar medium. We first consider the possibility that the power of the explosion is different into different directions, but the interstellar medium has spherical symmetry. Using the constant age of all parts of the remnant and the scaling laws of the self-similar model (see e.g. Kaastra & Jansen 1992) it is possible to show that in this case the observed reduced emission measure ratio C_{SW}/C_{NE} of 5 results into a shock radius ratio R_{SW}/R_{NE} of $5^{1/3}=1.71$ for $s=0$ and 0.2 for $s=2$. Both values are clearly not in agreement with the observed X-ray image (Pisarski et al. 1984), hence a different explosion energy into different directions seems unlikely.

Another possibility is that the explosion energy does not depend upon direction, but the interstellar medium density does. In that case it can be shown that the shock radius of the SW part is 0.79 of the NE shock radius (for an observed emission measure ratio of 5 as above). This seems to be in agreement with the X-ray image, which shows a slightly smaller curvature radius for the SW part as compared to the dimmer NE part. The pre-shock density in the SW part must then be a factor of 3.2 larger than in the NE part. In our analysis of mainly the SW part we have adopted a shock radius θ of 21′. Correcting for a different shock radius in the NE and SW part as suggested above, leads to a value of $\theta_{SW} = 18\overset{\prime}{.}5$. Since the SW part fills only 6.3% of the remnant (Table 2) we obtain slightly revised values for the ejected and swept-up mass: 22 and $8 M_\odot$ respectively. The explosion energy remains unaltered, while the distance to the remnant is now slightly larger: 0.95 ± 0.4 pc.

4. Conclusions

The present X-ray spectrum of RCW 86 allows for the first time a reliable estimate of the ionisation parameter $U = \int n_e \, dt$. The spectrum is consistent with the adiabatic reverse shock model of Chevalier (1982) with $s=2$. The best fit is obtained for n near 12, but all other possible values down to $n=5$ (the Sedov $s=2$ limit) cannot be excluded. Isothermal models or adiabatic models with $s=0$ are excluded, unless very small filling factors (<0.01) are accepted.

The best fit spectrum is consistent with a type II supernova explosion with about 2 10^{44} J of explosion energy. The progenitor had a mass of at least $22 M_\odot$ and went off in a medium with density $\propto r^{-2}$. The present pre-shock hydrogen density is 0.24 cm^{-3}. The distance to RCW 86 derived is 0.95 ± 0.4 pc. The abundances of Si, S and Fe are below the solar values, consistent with information obtained from optical line emission.

Acknowledgements. The present observation of RCW 86 was made during the PV phase of Ginga. We thank the Ginga Team for providing us with the data. J.S. Kaastra thanks staff and students of the Astrophysics Department of Nagoya University for their hospitality during his stay at Nagoya. The Laboratory for Space Research Leiden is supported financially by NWO, the Netherlands Organization for Scientific Research.

References

Anders E., Grevesse N., 1989, Geochimica et Cosmochimica Acta 53, 197

Band D.L., 1988, ApJ 332, 842

Chevalier R.A., 1982, ApJ 258, 790

Claas J.J., Smith A., Kaastra J.S., de Korte P.A.J., Peacock A., 1989, ApJ 337, 399

Clark D.H., Stephenson F.R., 1977, Historical Supernovae. Pergamon, Oxford

Hamilton A.J.S., Sarazin C.L., 1984, ApJ 284, 601

Hayashida K., Inoue H., Koyama K., et al., 1989, PASJ 41, 373

Huang Y.-L., Moriarty-Schieven G.H., 1987, Sci 235, 59
Jansen F.A., Smith A., Bleeker J.A.M., et al., 1988, ApJ 331, 949
Kaastra J.S., Jansen F.A., 1992, A&A (in press)
Koyama K., Makishima K., Tanaka Y., Tsunemi H., 1986, PASJ 38, 121
Leibowitz E.M., Danziger I.J., 1983, MNRAS 204, 273
Masai K., 1984, Ap&SS 98, 367
Morrison R., McCammon D., 1983, ApJ 270, 119
Naranan S., Shulman S., Yentis D., Fritz G., Friedman H., 1977, ApJ 213, L53
Nugent J.J., Pravdo S.H., Garmire G.P., et al., 1984, ApJ 284, 612
Pisarski R.L., Helfand D.J., Kahn S.M., 1984, ApJ 277, 710
Ruiz M.T., 1981, ApJ 243, 814
Sedov L., 1959, Similarity and Dimensional Methods in Mechanics. Academic Press, New York
Solinger A., Rappaport S., Buff J., 1975, ApJ 201, 159
Turner M.J.L., Thomas H.D., Patchett B.E., et al., 1989, PASJ 41, 345
Warwick R.S., Turner M.J.L., Watson M.G., Willingale R., 1985, Nat 317, 218
Winkler P.F., 1978, ApJ 221, 220
Yamauchi S., 1991, Ph.D. Thesis, Nagoya University